Spin-orbit coupling and crystal-field distortions for a low-spin $3d^5$ state in $BaCoO_3$

Y. Y. Chin,[1,2] Z. Hu,[3] H.-J. Lin,[2] S. Agrestini,[3] J. Weinen,[3] C. Martin,[4] S. Hébert,[4] A. Maignan,[4] A. Tanaka,[5] J. C. Cezar,[6] N. B. Brookes,[6] Y.-F. Liao,[2] K.-D. Tsuei,[2] C. T. Chen,[2] D. I. Khomskii,[7] and L. H. Tjeng[3]

[1]*Department of Physics, National Chung Cheng University, 168, Section 1, University Road, Min-Hsiung, Chiayi 62102, Taiwan*
[2]*National Synchrotron Radiation Research Center, 101 Hsin-Ann Road, Hsinchu 30076, Taiwan*
[3]*Max Planck Institute for Chemical Physics of Solids, Nöthnitzer Straße 40, 01187 Dresden, Germany*
[4]*Laboratoire CRISMAT, Normandie Univ, ENSICAEN, UNICAEN, CNRS, 14050 Caen, France*
[5]*Department of Quantum Matter, ADSM, Hiroshima University, Higashi-Hiroshima 739-8530, Japan*
[6]*European Synchrotron Radiation Facility, 71 Avenue des Martyrs, 38043 Grenoble, France*
[7]*Institute of Physics II, University of Cologne, Zülpicher Straße 77, 50937 Cologne, Germany*

(Received 22 May 2019; published 26 November 2019)

We have studied the electronic structure of $BaCoO_3$ using soft x-ray absorption spectroscopy at the Co $L_{2,3}$ and O K edges, magnetic circular dichroism at the Co $L_{2,3}$ edges, and valence band hard x-ray photoelectron spectroscopy. The quantitative analysis of the spectra established that the Co ions are in the formal low-spin tetravalent $3d^5$ state and that the system is a negative charge transfer Mott insulator. The spin-orbit coupling also plays an important role for the magnetism of the system. At the same time, a trigonal crystal field is present with sufficient strength to bring the $3d^5$ ion away from the $J_{\text{eff}} = 1/2$ state. The sign of this crystal field is such that the a_{1g} orbital is doubly occupied, explaining the absence of a Peierls transition in this system, which consists of chains of face-sharing CoO_6 octahedra. Moreover, with one hole residing in e_g^{π}, the presence of an orbital moment and strong magnetocrystalline anisotropy can be understood. Yet we also infer that crystal fields with lower symmetry must be present to reproduce the measured orbital moment quantitatively, thereby suggesting the possibility for orbital ordering to occur in $BaCoO_3$.

DOI: 10.1103/PhysRevB.100.205139

I. INTRODUCTION

Cobalt oxides have generated considerable attention in the scientific community due to their complex and large diversity of physical phenomena, such as metal-insulator transitions [1–3], superconductivity [4–7], large magnetoresistance [8], high thermoelectric power [2,9,10], and also high catalytic activity for energy storage applications [11–14]. This richness of electronic and magnetic properties is closely related not only to the possibility of stabilizing cobalt in different valence states but also to the so-called spin-state degree of freedom [15–21]. For example, in an octahedral coordination, Co^{3+} and Co^{4+} ions, which have the formal d^6 and d^5 configurations, respectively, can exist in three possible spin states: a high-spin (HS) state, a low-spin (LS) state, and even an intermediate-spin (IS) state.

$BaCoO_3$ is a fascinating cobalt oxide with various intriguing aspects. The crystal structure consists of one-dimensional (1D) c-axis chains of face-sharing CoO_6 octahedra forming a two-dimensional (2D) triangular lattice in the ab plane [22–24]. $BaCoO_3$ can be considered to belong to the material class of $A_{n+2}Co_{n+1}O_{3n+3}$ (A=Ca, Sr, Ba, $n \to \infty$) [25–27]. Depending on n and on the A ion, the competition between the 1D and 2D interactions in this material class can generate peculiar transport and magnetic properties such as successive magnetic transitions [28,29] and magnetization plateaus [30–34], unusually large magnetocrystalline anisotropy [35], and collinear-magnetism-driven ferroelectricity [36], as well as the phenomenon of quantum tunneling of the magnetization [33].

The high-temperature magnetic susceptibility of $BaCoO_3$ shows an effective magnetic moment of $2.3\mu_B$, which was taken to be a sign of the existence of LS Co^{4+} [24,37], although it is larger than the spin-only value of $1.73\mu_B$ for an $S = 1/2$ ion. Neutron powder diffraction (NPD) [29] and muon spin rotation (μSR) experiments [25,29] indicated the presence of a three-dimensional antiferromagnetic (AFM) coupling below $T_N = 15$ K. Between 15 and 53 K, 2D ferromagnetism takes place, and above 53 K there is superparamagnetism followed by the Curie law for temperatures above 250 K [25,26,29]. The magnetic Bragg reflections in NPD can be indexed with ferromagnetic (FM) coupling intrachain and AFM coupling between the chains with a propagation vector $k = (1/3, 1/3, 0)$ [29] and a magnetic moment of $0.53\mu_B$, suggesting a geometric frustration for the triangular lattice in the ab plane.

$BaCoO_3$ is a small-gap semiconductor based on temperature-dependent resistivity measurements [23,24,37]. It is actually quite remarkable that it is not metallic. In view of the very high formal oxidation state of 4+, one may expect that the oxygen $2p$ to cobalt $3d$ charge transfer energy is negative and that the system should show a p-type metallic behavior according to the Zaanen-Sawatzky-Allen phase diagram [38]. This apparently does not happen and is thus different from, for example, $SrCoO_3$ [18], also an octahedral Co^{4+} system, which indeed shows a metallic signature in its resistivity.

Several *ab initio* band structure calculations have been carried out to explain the physical properties of $BaCoO_3$

[39–45]. It was concluded that a Peierls transition in the 1D *c*-axis chain is unlikely to be the reason for the insulating state [45]. Later calculations took into account electron correlation effects at the Co sites in the so-called local-density approximation (LDA) + U approach [40–44] to reproduce the insulating state and to explain the magnetic structure. These calculations also proposed that the total energy of the system can be lowered if an orbital ordering is allowed to occur within the *c*-axis chain.

In view of the recent frantic search for the materialization of quantum spin liquids and Kitaev model based on Ir and Ru compounds with the LS octahedral d^5 configuration [46–48], it would be useful to know whether the spin-orbit interaction of the Co ion can also stabilize the $J_{\text{eff}} = 1/2$ state in $BaCoO_3$. Interestingly, $BaCoO_3$ was also mentioned explicitly in recent theoretical studies [49,50] as a candidate material for SU(4) physics to occur: a system with a highly symmetric Hamiltonian containing orbital and spin interactions of the Heisenberg type [51–53] showing, for example, gapless spin and orbital waves.

Our objective here is to determine experimentally, using x-ray absorption spectroscopy (XAS) and x-ray magnetic circular dichroism (XMCD), the local electronic structure of the Co ions in $BaCoO_3$. In particular, we aim to determine the charge, spin, and orbital state of Co and its relation to the local coordination and crystal structure. We also need to determine spectroscopically that the material is an insulator in order to provide justification for the various approximations to model its magnetic properties. With this we hope to shed light on why there is no Peierls distortion in this system, why the measured effective magnetic moment deviates from the spin-only value, and whether the conditions for a $J_{\text{eff}} = 1/2$ state, for the orbital ordering or for other orbital physics phenomena as proposed by the theoretical studies mentioned above, can be met.

II. EXPERIMENTS

The $BaCoO_3$ ceramics were prepared using a two-step process as described elsewhere [27]. The Co $L_{2,3}$ and the O K XAS spectra were measured in the total electron yield mode (TEY) at the Dragon beamline of the National Synchrotron Radiation Research Center (NSRRC) in Taiwan. The measurements were carried out at room temperature. The Co $L_{2,3}$ XMCD spectra were recorded at the ID8 beamline of the European Synchrotron Radiation Facility in Grenoble under a magnetic field of 5 T at 50 K. Below 50 K, the sample became strongly charged and could not be measured in the TEY mode, indicating insulating properties. CoO and NiO single crystals were measured simultaneously in another chamber for energy calibration.

The hard x-ray photoelectron spectroscopy (HAXPES) experiment was carried out at the Max Planck-NSRRC end station at the Taiwan undulator beamline BL12XU at SPring-8 in Hyogo, Japan. The photon beam was linearly polarized with the electrical field vector in the plane of the storage ring (i.e., horizontal), and the photon energy was set at about 6.5 keV. The experimental setup has two MB Scientific A-1 HE analyzers. We used the analyzer which was mounted vertically. The direction of the photoelectrons was thus perpendicular to the electrical field vector and the Poynting vector of the beam. The overall energy resolution was 0.35 eV, and the Fermi level was calibrated using polycrystalline gold. The $BaCoO_3$ sample was cleaved *in situ* in order to have a clean surface. The measurements were done at room temperature.

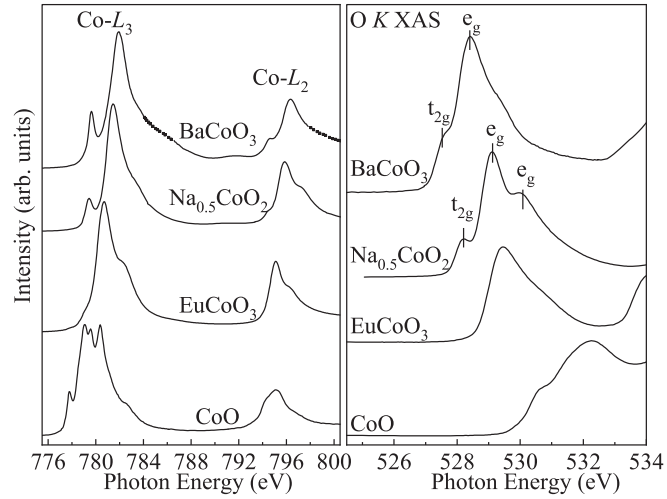

FIG. 1. Left: Experimental Co $L_{2,3}$ XAS spectra of $BaCoO_3$, $Na_{0.5}CoO_2$ (from Ref. [54]), $EuCoO_3$ (from Ref. [55]), and CoO. Right: Experimental O K XAS spectra of $BaCoO_3$, $Na_{0.5}CoO_2$ (from Ref. [54]), $EuCoO_3$ (from Ref. [55]), and CoO.

III. RESULTS AND DISCUSSION

A. Valence state and orbital occupation

In Fig. 1 (left panel), we present the Co $L_{2,3}$ XAS spectra of $BaCoO_3$ taken at room temperature together with those of $Na_{0.5}CoO_2$ (from Ref. [54]) as a $Co^{3.5+}$ reference, $EuCoO_3$ (from Ref. [55]) as a Co^{3+} reference, and CoO as a Co^{2+} reference. For the spectrum of $BaCoO_3$, we have removed the Ba $M_{4,5}$ white lines located at 784 and 798 eV using the Ba $M_{4,5}$ spectrum of $BaFeO_3$ (from Ref. [56]; see the Appendix). It is well known that XAS spectra at the 3d transition-metal $L_{2,3}$ edges are highly sensitive to the valence state: an increase of the valence state of the metal ion causes a shift of the XAS $L_{2,3}$ spectra towards higher energies [35,57]. In Fig. 1, we can clearly observe a shift of the center of gravity of the L_3 spectrum to higher photon energies from CoO to $EuCoO_3$ to $Na_{0.5}CoO_2$ and to $BaCoO_3$ by about 1 eV each time. This observation indicates that the formal valence of the Co ions in $BaCoO_3$ is 4+.

By studying the O K XAS, we can check the valence state and, furthermore, also identify the occupied orbitals of the Co ions in $BaCoO_3$. In Fig. 1 (right panel), the structures from 528 to 533 eV are due to transitions from the O 1s core level to the O 2p orbitals which are hybridized with the unoccupied Co 3d t_{2g} and e_g states. From the bottom to the top, one can see a gradual shift of the preedge peak in the O K XAS spectra to lower energies for an increase of the formal valence from Co^{2+} in CoO to Co^{3+} in $EuCoO_3$ [55] to $Co^{3.5+}$ in $Na_{0.5}CoO_2$ [54] and further to Co^{4+} in $BaCoO_3$. This energy lowering of the preedge peak reflects the increase of the valence state

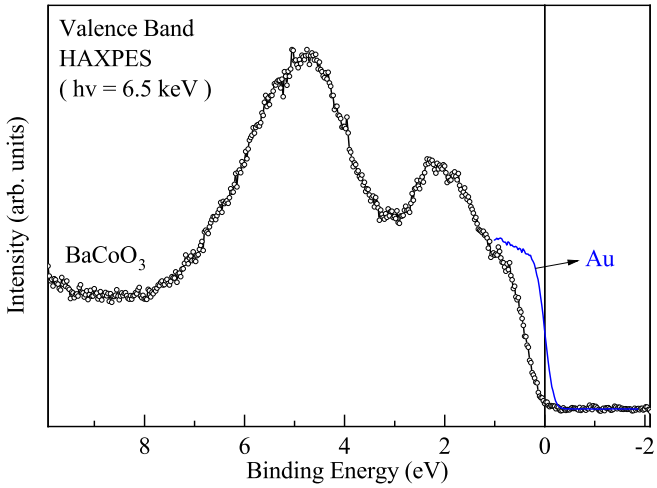

FIG. 2. Valence band HAXPES spectra of $BaCoO_3$ (black circles) and Au (blue curve) for energy calibration.

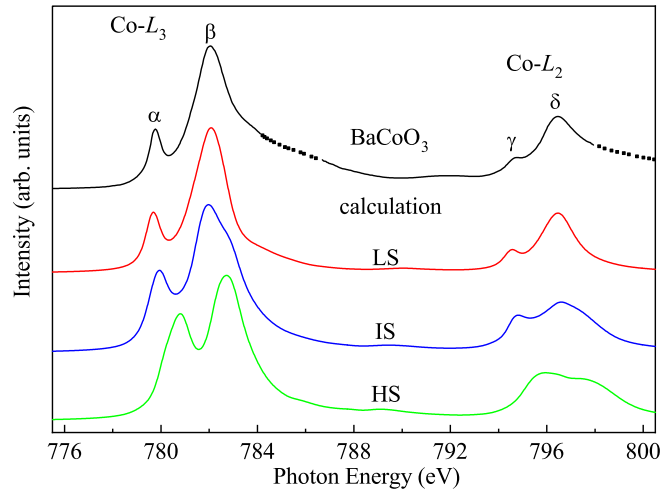

FIG. 3. Calculated Co $L_{2,3}$ XAS spectra for a CoO_6 cluster with the $3d^5$ low-spin (LS), intermediate-spin (IS), and high-spin (HS) state configurations. The O $2p$ to Co $3d$ charge transfer energy in the calculations is negative: −3.5 eV. Characteristic features of the experimental spectrum are labeled with α, β, γ, and δ to facilitate the discussion.

of transition-metal ions in oxides, as known from previous studies [58–60].

The preedge peak structure of the O K XAS also provides information about the orbital occupations and the possible spin states. The main peak of the $EuCoO_3$ spectrum at 529.5 eV can be assigned to transitions to the fourfold-degenerate e_g holes of the LS Co $3d^6$ configuration. The extra peak appearing at the lower energy of 528.2 eV in $Na_{0.5}CoO_2$ [54] and 527.5 eV for $BaCoO_3$ can then be assigned to the presence of an additional hole in the t_{2g} shell. This implies that the Co^{4+} ion has the LS configuration: with one t_{2g} and four e_g holes, the electron orbital occupation is t_{2g}^5. The slight energy shift to lower photon energies in the spectrum of $BaCoO_3$ with respect to that of $Na_{0.5}CoO_2$ reflects the higher valence state of Co in the former. We would like to note that the O K XAS spectrum of $BaCoO_3$ is quite different from that of $La_{1-x}Sr_xCoO_3$, which has a different orbital occupation and therefore different spin state (IS) for its Co^{4+} ions [61], confirming our analysis. The orbital occupation and the LS state in $BaCoO_3$ are consistent with the very short Co-O distance of 1.874 Å in it [22].

B. Presence of band gap

The valence band spectrum of $BaCoO_3$ taken with the bulk-sensitive HAXPES method is displayed in Fig. 2. The Fermi edge of Au metal is also measured to serve as a reference. The most relevant information that we would like to extract from this room temperature spectrum is that the spectral weight of $BaCoO_3$ at the Fermi level is negligible. This agrees well with the semiconducting behavior as observed in resistivity measurements [23,24,37]. Comparing the leading edge of the $BaCoO_3$ valence band with the Au Fermi edge, we can estimate that the band gap is about 0.3 eV. Here we assume that the bottom of the conduction band is pinned at the Fermi level. The true band gap value could, of course, be larger if the Fermi level is pinned by in-gap states, but at the moment we have no information about the energy position of the bottom of the conduction band. Despite these uncertainties, we can safely conclude that $BaCoO_3$ is truly an insulating material with a band gap of several tenths of an eV.

The finding of a band gap is important for the quantitative modeling of the local electronic structure of $BaCoO_3$. We now can meaningfully use a single-site configuration interaction approach which includes the effect of the lattice on the local Co ion by taking only an effective CoO_6 cluster. Such a single-site approach may not be valid if the system is a metal with substantial intersite or intercluster charge fluctuations. As mentioned above, a p-type metal behavior could be envisioned within the Zaanen-Sawatzky-Allen phase diagram [38] for high-oxidation-state transition-metal oxides. Apparently, this does not materialize for $BaCoO_3$, probably due to the fact that the ligand holes have poor intersite or intercluster hopping integrals due to the face-sharing nature of the CoO_6 octahedra. Here one can envision that an O $2p$ orbital which is π bonded to the t_{2g} orbital of a particular Co site has poor π bonding with the t_{2g} orbital of the neighboring Co due to the fact that the Co-O-Co bond angle of about 78° [22,62] is not too far from 90°. The situation for oxides consisting of corner-sharing octahedra, e.g., $SrCoO_3$ [18,63,64] and Sr_2CoO_4 [65,66], is clearly different.

C. Charge transfer energy and spin state

We now analyze quantitatively the Co $L_{2,3}$ XAS spectrum of $BaCoO_3$ from Fig. 1 (left panel, top curve) using a CoO_6 cluster model which includes configuration interaction and full atomic multiplet theory [67,68]. It is well known that $L_{2,3}$ XAS is sensitive not only to the charge and orbital states but also to the spin state [19,55]. Figure 3 depicts the results. Here we have calculated the spectra for a $Co^{4+}O_6$ cluster with the $3d^5$ LS, IS, and HS state configurations [69]. We can clearly observe that the LS scenario gives by far the best match to the experimental spectrum. The energy positions and intensities of the characteristic features labeled α, β, γ, and δ are all

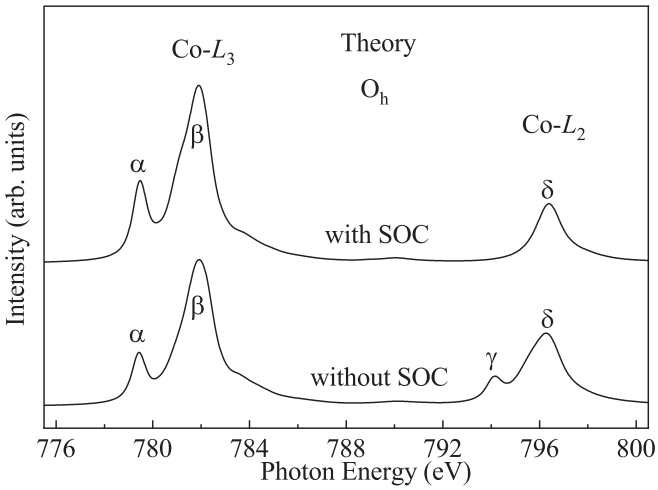

FIG. 4. Calculated Co $L_{2,3}$ XAS spectra for a CoO_6 cluster with the $3d^5$ LS configuration in O_h symmetry, with and without spin-orbit coupling (SOC).

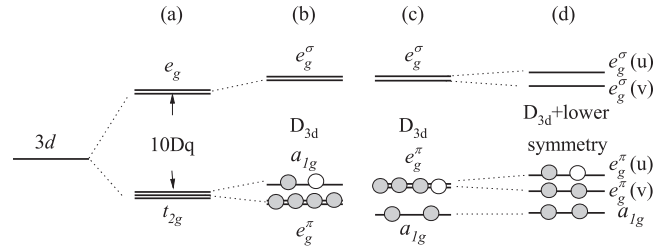

FIG. 5. Schematic one-electron energy level diagram of a CoO_6 cluster in $BaCoO_3$. (a) In O_h coordination the levels are given by the t_{2g} and e_g subshells split by an energy $10Dq$. In the presence of a D_{3d} trigonal distortion, the levels are labeled e_g^π, a_{1g}, and e_g^σ, whereby for (b) a positive trigonal crystal-field splitting the LS d^5 configuration is characterized by a fully occupied e_g^π and one hole in a_{1g}, and for (c) a negative splitting the LS d^5 configuration is described by a fully occupied a_{1g} and one hole in e_g^π. (d) Adding a local lower-symmetry distortion splits the levels further into five doublets which carry the labels a_{1g}, $e_g^\pi(u)$, $e_g^\pi(v)$, $e_g^\sigma(u)$, and $e_g^\sigma(v)$.

well reproduced. This establishes firmly that the Co ion is in the formal $S = 1/2$ t_{2g}^5 type of configuration, fully consistent with the O K-edge analysis above. The stabilization of the LS state can be attributed to a large effective crystal or ligand field interaction due to the relatively short Co-O distance of 1.874 Å. This is to be contrasted with, for example, $SrCoO_3$, which has a larger Co-O distance of 1.918 Å and has an IS-like ground state [18,63].

To achieve good agreement between theory and experiment, it is important to use a negative value for the O $2p$ to Co $3d$ charge transfer energy in the calculation: we have taken -3.5 eV. This means that the main charge configuration of Co is not $3d^5$ (8% weight) but mainly $3d^6\underline{L}$ (45%) and $3d^7\underline{L}^2$ (40%) with even some $3d^8\underline{L}^3$ (7%). Here $\underline{L}$ denotes a hole in the O $2p$ ligands. The formal valence and the local symmetry of the Co system are, nevertheless, still those of Co^{4+}.

In the next sections we will explain further important details that we were able to extract from the calculations, in particular about the effect of the spin-orbit coupling (SOC) and low-symmetry crystal-field interactions determining the magnetic properties as well as the absence of a Peierls distortion.

D. Spin-orbit interaction in a d^5 system

We first assume a pure O_h coordination for the CoO_6 cluster and calculate the Co $L_{2,3}$ XAS spectrum in the LS state scenario. We have done this calculation with the SOC constant set at the atomic value of $\zeta_{SOC} = 65$ meV and also with the SOC constant set to zero. The result is shown in Fig. 4. We can see that features α, β, and δ are present for both cases, but we can also see a large difference with respect to feature γ. Without the SOC, the L_2 white line contains the prepeak structure γ, while such a prepeak is completely absent when the SOC is included. Interestingly, the experimental L_2 white line of $BaCoO_3$ does contain such a prepeak, although it is not as strong as in the scenario where the SOC is switched off.

We now concentrate on the cause of the presence or absence of prepeak γ. The LS ground state of a d^5 ion in O_h symmetry is given by the t_{2g}^5 orbital configuration. The presence of SOC converts this into an effective $J_{\text{eff}} = 1/2$ state, a ground state that one may hope to find in Ir^{4+} and Ru^{3+} compounds [46,47]. It was already noticed early on for LS O_h-coordinated $4d^5$ transition-metal compounds that the L_2 edge does not have a prepeak γ [68,70]. The explanation is that the matrix element is zero for the $2p$ to t_{2g} transition at the L_2 edge if the ground state is $J_{\text{eff}} = 1/2$ [70,71]. Switching off the SOC and thus abandoning $J_{\text{eff}} = 1/2$ allow this matrix element to become nonzero and thus prepeak γ to appear, as we can see in Fig. 4.

We thus can conclude that the presence of a prepeak γ in the experimental $L_{2,3}$ XAS spectrum implies that $BaCoO_3$ is not a $J_{\text{eff}} = 1/2$ system. This in turn means that the effect of the SOC must be superseded by a strong crystal field with a symmetry lower than O_h.

E. Crystal fields: I. D_{3d}

In lowering the local symmetry of the Co ion from a pure O_h, we will first consider a D_{3d} trigonal distortion as this is suggested most naturally from the crystal structure. As depicted in Fig. 5, where we do not include the influence of the SOC, the one-electron crystal or ligand field energy levels carry the e_g^π, a_{1g}, and e_g^σ labels in D_{3d} instead of t_{2g} and e_g in O_h. Here we show two scenarios: one in which the a_{1g} orbital is higher in energy (more unstable) than e_g^π, which should be associated with a positive trigonal crystal-field splitting, and one where e_g^π is higher, which thus indicates a negative splitting. For a LS d^5 configuration, a positive splitting would result in a fully occupied e_g^π and one hole in a_{1g}, while a negative splitting would stabilize a fully occupied a_{1g} and one hole in e_g^π.

The crystal-field splitting in D_{3d} symmetry is determined by the crystal-field parameter $\triangle D_{3d}$ and the mixing parameter V_{mix}. $\triangle D_{3d}$ is the energy difference between the a_{1g} and $t_{2g}(u, v)$ orbitals, where $t_{2g}(u) = \sqrt{2/3}d_{x^2-y^2} - \sqrt{1/3}d_{xz}$ and $t_{2g}(v) = \sqrt{2/3}d_{xy} + \sqrt{1/3}d_{yz}$. V_{mix} describes the mixing between $t_{2g}(u, v)$ and $e_g(u, v)$, i.e., $V_{\text{mix}} =$

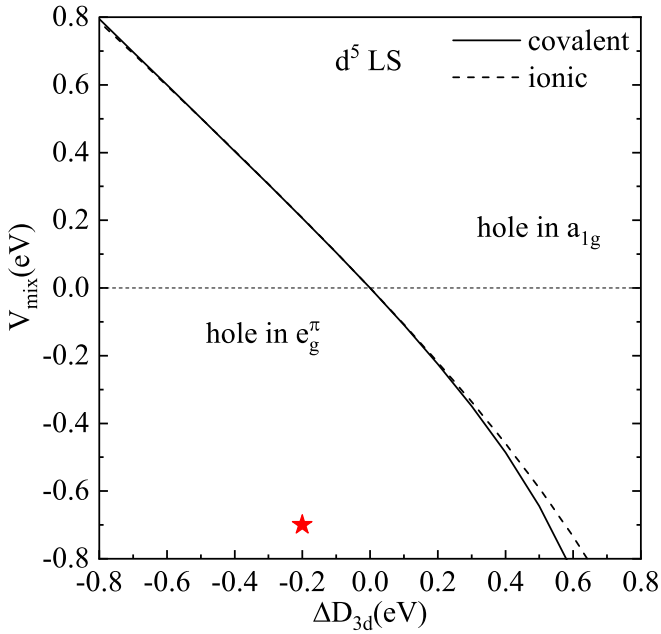

FIG. 6. Phase diagram for a low-spin Co^{4+} t_{2g}^5 configuration in D_{3d} symmetry, displaying the character of the hole occupation as a function of the crystal-field parameter $\triangle D_{3d}$ and the mixing parameter $V_{\rm mix}$. The phase diagram has been calculated with the spin-orbit coupling set to zero and for covalent (solid line as the boundary) and ionic (dashed line) scenarios; see text for further details. The red star in the phase diagram indicates the values for $\triangle D_{3d}$ and $V_{\rm mix}$ needed to reproduce the experimental XAS and XMCD spectra of $BaCoO_3$.

$\langle t_{2g}(u,v)|H|e_g(u,v)\rangle$, where $e_g(u) = \sqrt{1/3}d_{x^2-y^2} + \sqrt{2/3}d_{xz}$ and $e_g(v) = \sqrt{1/3}d_{xy} - \sqrt{2/3}d_{yz}$. The presence of $V_{\rm mix}$ leads to the formation of the $e_g^\pi(u,v)$ and $e_g^\sigma(u,v)$ orbitals (see also Refs. [54,72,73]).

We have calculated the sign of the splitting as a function of these two parameters and display the result in Fig. 6. We can clearly see that for negative $\triangle D_{3d}$ and negative $V_{\rm mix}$ the hole will be in e_g^π, while for positive $\triangle D_{3d}$ and positive $V_{\rm mix}$ it will be in a_{1g}. The calculations have been done with the SOC set to zero. The solid line represents the border between e_g^π and a_{1g} hole situations in a calculation taking into account the covalency and negative charge transfer energy, while the dashed line is the border in an ionic calculation where the LS state is artificially stabilized by taking a sufficiently large O_h crystal-field splitting.

In trying to determine the values of $\triangle D_{3d}$ and $V_{\rm mix}$ for $BaCoO_3$ from the experimental XMCD spectra, we have carried out cluster calculations where we have switched on the SOC, i.e., set it to its atomic value. However, it turned out that we were not able to find a satisfactory match between the experimental spectra and the simulations within the D_{3d} symmetry. A representative set of the "not satisfactory" simulations can be found in the Appendix. We found out that we need to lower the local symmetry of the Co ion even further.

F. Crystal fields: II. Lower symmetry

Figure 7(a) shows the overlay of the experimental XAS spectrum of $BaCoO_3$ and the simulation which includes a

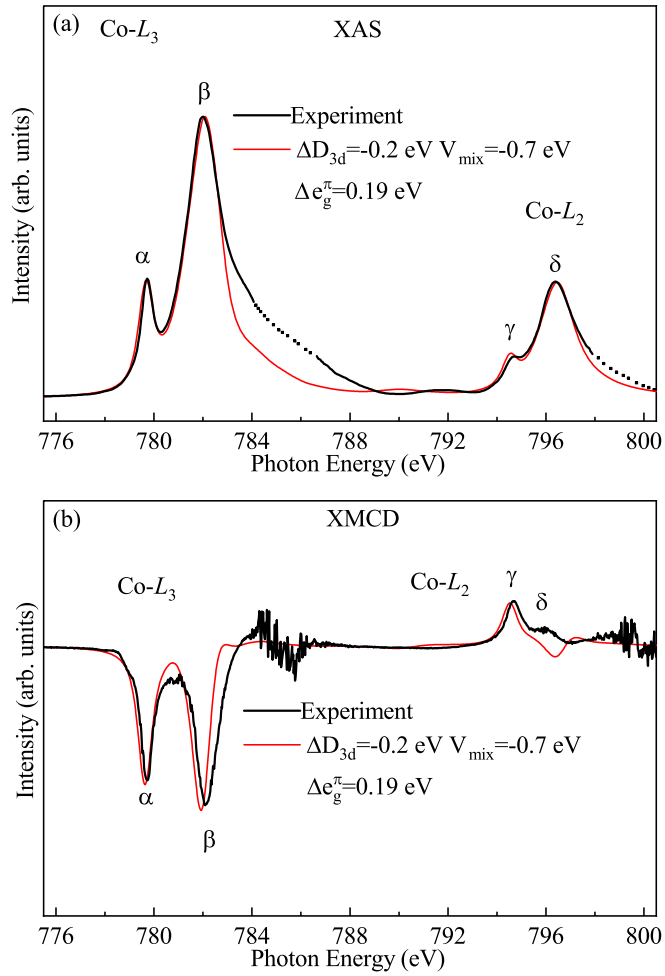

FIG. 7. Experimental Co $L_{2,3}$ (a) XAS and (b) XMCD spectra of $BaCoO_3$ (black lines and dots) together with simulations (red lines) using a CoO_6 cluster with the $3d^5$ LS configuration which includes a trigonal crystal field and lower-symmetry crystal field; see text.

low-symmetry crystal field that splits the e_g^π level into $e_g^\pi(u)$ and $e_g^\pi(v)$ by about 0.19 eV. The SOC in this calculation is set to its atomic value. We now can observe very good agreement between the simulation and experiment. The D_{3d} parameters that we used are $\triangle D_{3d} = -0.2$ eV and $V_{\rm mix} = -0.7$ eV. We are thus deep in the phase where the hole is e_g^π according to Fig. 6. This result is somewhat surprising since the trigonal distortion corresponds to the elongation of the octahedron along the c axis, so one may actually expect to have a positive trigonal crystal-field splitting. Apparently, longer-range interactions, due to, e.g., the presence of highly charge positive (4+) nearest-neighbor Co ions in the c-axis chain, have a greater influence and, in the end, make the trigonal crystal field effectively negative.

Looking in detail at the L_2 white line, we can observe that the prepeak γ can be reproduced in the simulation. So unlike in a pure O_h symmetry, the trigonal crystal field causes a mixing between the $J_{\rm eff} = 1/2$ and $J_{\rm eff} = 3/2$ states, and this mixing is strong enough that the prepeak γ indeed can show up in the spectrum. This, in turn, reiterates that $BaCoO_3$ is not a $J_{\rm eff} = 1/2$ system.

Figure 7(b) displays the XMCD spectrum taken at 50 K with a 5-T magnetic field (black lines and dots). The XMCD signal is pronounced, and it is remarkable that the intensity at the L_3 white line is heavily negative, while that at L_2 is only moderately positive. Using the XMCD sum rules developed by Thole *et al.* [74,75], we find $L_z/(2S_z + 7T_z) = 0.4$, so that we can directly infer that the negative value for the integrated XMCD intensity is indicative of the presence of an appreciable orbital contribution to the Co magnetic moment. This directly explains why the high-temperature magnetic susceptibility of $BaCoO_3$ shows an effective magnetic moment of $2.3\mu_B$ [24,37] that is larger than the spin-only value of $1.73\mu_B$ for an $S = 1/2$ ion.

Figure 7(b) also shows the simulation for the XMCD using the same parameter set as for the XAS in Fig. 7(a). The agreement between simulation and experiment is also very good for the XMCD. We therefore can safely conclude that we have found the proper set of parameter values for $BaCoO_3$.

We would like to note that our finding for the presence of the hole in the e_g^π orbital is in direct agreement with the orbital moment found from the XMCD since the opposite scenario in which the hole is in a_{1g} will, in an ionic picture, not produce an orbital moment. This can be explained as follows. In the presence of the SOC, we can make use of the $t_{2g}(\pm)$ orbitals defined as $t_{2g}(\pm) = \{\mp t_{2g}(u) - it_{2g}(v)\}/\sqrt{2}$, which denote the $l_z = \pm 1$ eigenstates of the pseudo $l = 1$ orbital moment within the t_{2g} orbitals. Analogously, we can define $e_g(\pm) = \{\mp e_g(u) - ie_g(v)\}/\sqrt{2}$ (these do not carry an orbital moment) to arrive at $e_g^\pi(\pm)$ and $e_g^\sigma(\pm)$ orbitals after $V_{\rm mix}$ has done its work. It is then straightforward to see that $e_g^\pi(\pm)$, which are degenerate in the D_{3d} point group symmetry, do carry a large orbital momentum $\sim 1\mu_{\rm B}$ in the presence of SOC, while a_{1g} does not. Obviously, we need to caution here that for the highly covalent $BaCoO_3$ some small amount of orbital moment (less than $0.2\mu_B$–$0.3\mu_B$) will be present if the hole is in a_{1g} as a result of the negative charge transfer energy and thus the presence of the $d^6\underline{L}$ states.

We also need to point out that the presence of a low-symmetry crystal field, due to, e.g., a C_{2h} local monoclinic distortion of the CoO_6 octahedron, that splits the e_g^π level into $e_g^\pi(u)$ and $e_g^\pi(v)$ by about 0.19 eV is necessary to explain the XMCD orbital moment quantitatively. Without such a splitting, a hole in the degenerate e_g^π orbital would carry an orbital moment of $1.04\mu_B$. The simulation in Fig. 7(b) reveals that the orbital moment from the XMCD is about $0.61\mu_B$. Thus, the low-symmetry crystal field is necessary to moderate the effect of the SOC. Furthermore, the simulation finds an S_z of $0.50\mu_B$ and a T_z of $0.10\mu_B$, thus yielding a $L_z/(2S_z + 7T_z)$ value of 0.36, which is quite close to the experimental XMCD sum rule value of 0.4. The effective moment extracted from the simulation is temperature dependent due to the presence of SOC-related low-lying excited states. We find a low-temperature value of $2.31\mu_B$, in good agreement with $2.3\mu_B$ from the experiment.

G. Discussion

Our finding of a negative trigonal crystal field and thus a hole in the e_g^π orbital means that the a_{1g} orbital is doubly occupied. This has important consequences for the discussion about the presence or absence of a Peierls distortion in $BaCoO_3$. The classical Peierls distortion occurs for a one-dimensional metallic system if a doubling of a unit cell by forming dimers can lead to a total energy gain, thereby also opening up a band gap. The starting point or necessary condition is a metallic band before the distortion takes place. In our case, we find that the a_{1g} orbital which is directed along the one-dimensional c-axis chain is fully occupied; that is, there is no degeneracy left to make a metallic band with this a_{1g}. This implies that there cannot be a Peierls phenomenon occurring in $BaCoO_3$, at least not on the basis of the a_{1g} band. Our results support the findings from the LDA+U band structure calculations, i.e., calculations which include the effect of Coulomb interactions in the Co $3d$ shell [40–44]. Those calculations also found that a_{1g} is completely below the Fermi level, i.e., fully occupied. Calculations without taking into account the on-site Coulomb interaction [39,45], in contrast, produced an a_{1g} band that crosses the Fermi level, i.e., a metallic band. Our experiment therefore also clearly shows that the insulating nature of $BaCoO_3$ is due to Mott physics.

It is quite interesting that we have found the presence of a crystal field with a symmetry lower than D_{3d}, namely, to split the e_g^π levels so that the XAS and XMCD can be well reproduced in the simulations. This lifting of the degeneracy of the e_g^π orbitals would be compatible with the proposal by Pardo *et al.* of having an in-chain orbital ordering [40–44]. Perhaps the situation could be similar to that of $BaVS_3$ [76]. This aspect deserves further study using, for example, pair-density-function analysis [77] on powder samples and/or high-resolution x-ray diffraction measurements on single crystals.

IV. CONCLUSIONS

We have carried out a detailed study of the local electronic structure of $BaCoO_3$ using soft x-ray absorption, magnetic circular dichroism, and hard x-ray photoemission. We established that the Co ions are in the formal low-spin tetravalent $3d^5$ state and that this oxide is a negative charge transfer energy system. Remarkably, it is also a Mott insulator despite its negative charge transfer energy. Although the low-spin d^5 configuration could, in principle, produce a $J_{\rm eff} = 1/2$ state, we found that this has not materialized due to the presence of a strong trigonal crystal field. The sign of this crystal field is such that the a_{1g} orbital is doubly occupied, explaining the absence of a Peierls distortion in the c-axis chains. With one hole residing in the e_g^π subshell, the spin-orbit interaction becomes active, leading to the presence of an orbital moment which explains why the measured effective magnetic moment is larger than the spin-only value and why the system has a strong magnetocrystalline anisotropy. Interestingly, we also found that crystal fields with lower symmetry must be present to reproduce the measured orbital moment quantitatively. This then opens the possibility for orbital ordering to occur in $BaCoO_3$ as proposed by LDA+U calculations on $BaCoO_3$ [40–44] and $BaVS_3$ [76]. To what extent the system can be a SU(4) system or could show spiral orbital order [51–53] requires further detailed research.

ACKNOWLEDGMENTS

We would like to thank M. Haverkort for valuable discussions. We acknowledge the support by the Ministry of Science and Technology of the Republic of China through MOST 107-2112-M-194-001-MY3, by the Deutsche Forschungsgemeinschaft through SFB 1143 (project ID 247310070), and by the Max Planck-POSTECH-Hsinchu Center for Complex Phase Materials. The work of D.I.K. was funded by the Deutsche Forschungsgemeinschaft through SFB 1238 (Project ID 277146847).

APPENDIX

Figure 8 depicts the Co $L_{2,3}$ and Ba $M_{4,5}$ XAS spectra of $BaCoO_3$ together with the Ba $M_{4,5}$ XAS spectrum of $BaFeO_3$ from Ref. [56]. The difference between these two spectra reveals the pure Co $L_{2,3}$ spectrum of Co $L_{2,3}$ which is used and displayed in Figs. 1, 3, and 7.

Figure 9 shows the experimental XAS and XMCD spectrum of $BaCoO_3$ together with simulations using a CoO_6 cluster in the low-spin configuration. The SOC is set to its atomic value. The local coordination is D_{3d}, and the figure illustrates that a satisfactory agreement between experiment and simulation cannot be found for a wide range of parameters $\triangle D_{3d}$ and V_{mix} within this D_{3d} scenario. A symmetry lower than D_{3d} is required, as explained in the main text.

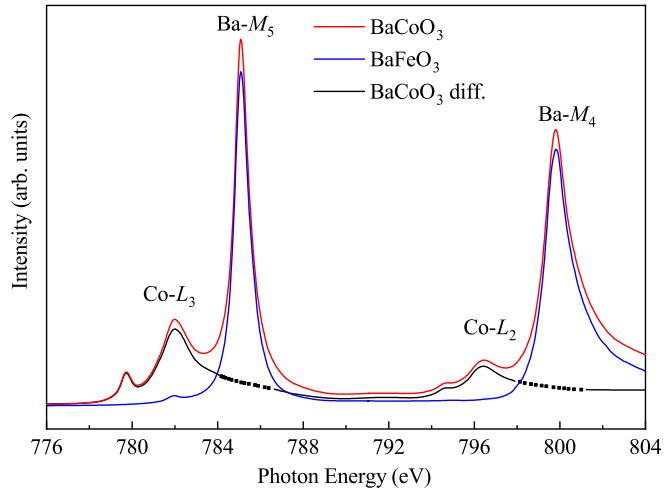

FIG. 8. Co $L_{2,3}$ and Ba $M_{4,5}$ XAS spectra of $BaCoO_3$ (red line) and the Ba $M_{4,5}$ XAS spectrum of $BaFeO_3$ (blue line) from Ref. [56]. The difference spectrum (black line) represents the pure Co $L_{2,3}$ XAS spectrum of $BaCoO_3$.

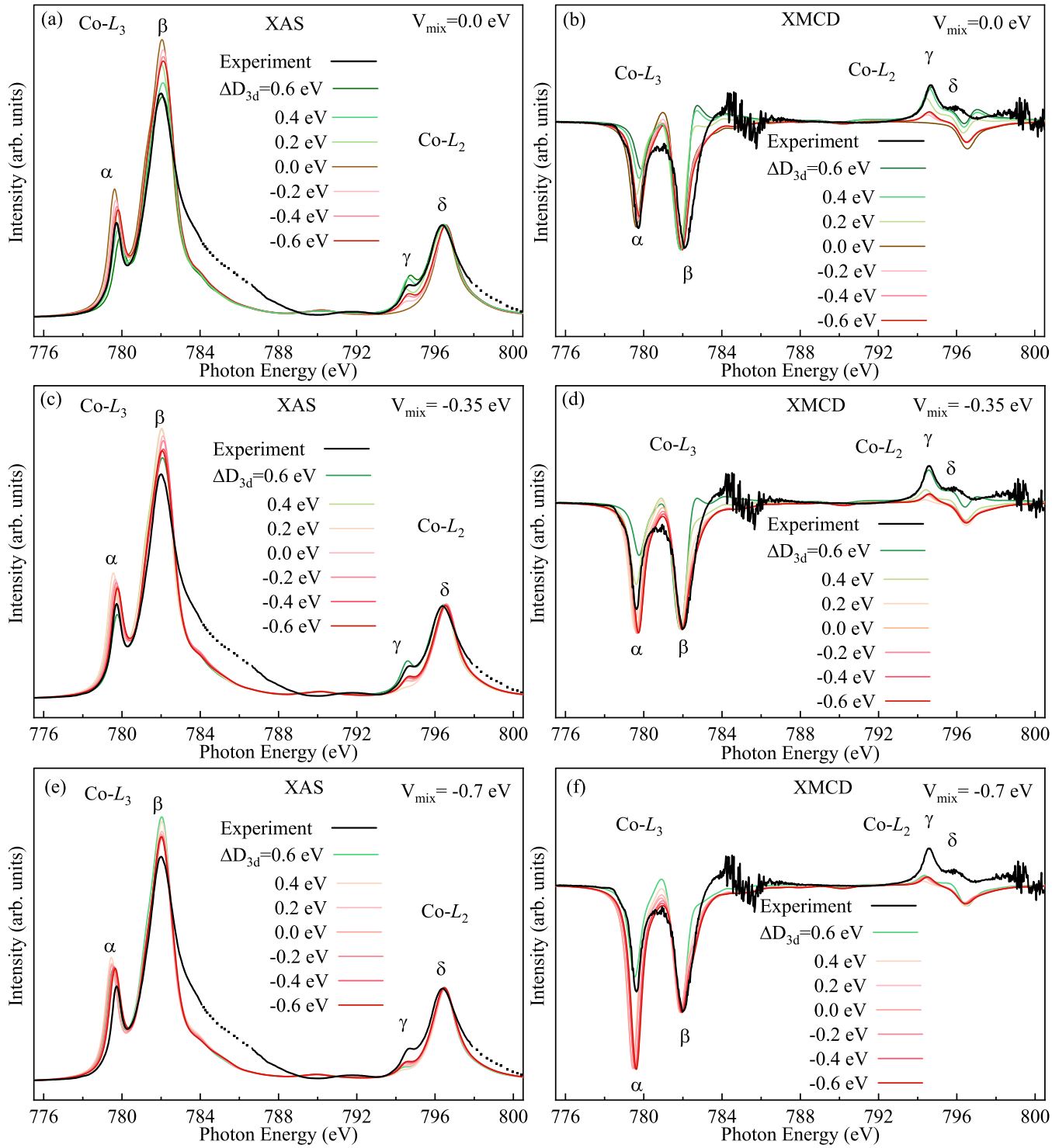

FIG. 9. Co $L_{2,3}$ XAS and XMCD spectra of $BaCoO_3$: experiment (black lines and dots) and simulations (colored lines). (a), (c), and (e) show the XAS, and (b), (d), and (f) show the XMCD data. The simulations were performed for (a) and (b) $V_{\rm mix} = 0.0$ eV, (c) and (d) -0.35 eV, and (e) and (f) -0.7 eV and $\triangle D_{3d}$ varying between -0.6 and $+0.6$ eV in steps of 0.2 eV.

[1] P. M. Raccah and J. B. Goodenough, First-order localized-electron ⇆ Collective-electron transition in $LaCoO_3$, Phys. Rev. **155**, 932 (1967).

[2] C. Martin, A. Maignan, D. Pelloquin, N. Nguyen, and B. Raveau, Magnetoresistance in the oxygen deficient $LnBaCo_2O_{5.4}$ (Ln=Eu, Gd) phases, Appl. Phys. Lett. **71**, 1421 (1997).

[3] M. Imada, A. Fujimori, and Y. Tokura, Metal-insulator transitions, Rev. Mod. Phys. **70**, 1039 (1998).

[4] R. E. Schaak, T. Klimczuk, M. L. Foo, and R. J. Cava, Superconductivity phase diagram of $Na_xCoO_2{\cdot}1.3H_2O$, Nature (London) **424**, 527 (2003).

[5] K. Takada, K. Fukuda, M. Osada, I. Nakai, F. Izumi, R. A. Dilanian, K. Kato, M. Takata, H. Sakurai, E. Takayama-Muromachi, and T. Sasaki, Chemical composition and crystal structure of superconducting sodium cobalt oxide bilayer-hydrate, J. Mater. Chem. **14**, 1448 (2004).

[6] K. Takada, H. Sakurai, E. Takayama-Muromachi, F. Izumi, R. A. Dilanian, and T. Sasaki, Superconductivity in two-dimensional CoO_2 layers, Nature (London) **422**, 53 (2003).

[7] H. Ohta, K. Yoshimura, Z. Hu, Y. Y. Chin, H.-J. Lin, H. H. Hsieh, C. T. Chen, and L. H. Tjeng, Determination of the Co Valence in Bilayer Hydrated Superconducting $Na_xCoO_2{\cdot}yH_2O$ by Soft X-Ray Absorption Spectroscopy, Phys. Rev. Lett. **107**, 066404 (2011).

[8] J. Pérez, J. García, J. Blasco, and J. Stankiewicz, Spin-Glass Behavior and Giant Magnetoresistance in the $(RE)Ni_{0.3}Co_{0.7}O_3$ (RE = La, Nd, Sm) System, Phys. Rev. Lett. **80**, 2401 (1998).

[9] I. Terasaki, Y. Sasago, and K. Uchinokura, Large thermoelectric power in $NaCo_2O_4$ single crystals, Phys. Rev. B **56**, R12685 (1997).

[10] A. C. Masset, C. Michel, A. Maignan, M. Hervieu, O. Toulemonde, F. Studer, B. Raveau, and J. Hejtmanek, Misfit-layered cobaltite with an anisotropic giant magnetoresistance: $Ca_3Co_4O_9$, Phys. Rev. B **62**, 166 (2000).

[11] J. Suntivich, K. J. May, H. A. Gasteiger, J. B. Goodenough, and Y. Shao-Horn, A perovskite oxide optimized for oxygen evolution catalysis from molecular orbital principles, Science **334**, 1383 (2011).

[12] W. Xu, J. Cai, J. Zhou, Y. Ou, W. Long, Z. You, and Y. Luo, Highly effective direct decomposition of nitric oxide by microwave catalysis over $BaMeO_3$ (Me=Mn, Co, Fe) mixed oxides at low temperature under excess oxygen, ChemCatChem **8**, 417 (2016).

[13] Y. Liang, Y. Li, H. Wang, J. Zhou, J. Wang, T. Regier, and H. Dai, Co_3O_4 nanocrystals on graphene as a synergistic catalyst for oxygen reduction reaction, Nat. Mater. **10**, 780 (2011).

[14] H. Jeen, W. S. Choi, M. D. Biegalski, C. M. Folkman, I.-C. Tung, D. D. Fong, J. W. Freeland, D. Shin, H. Ohta, M. F. Chisholm, and H. N. Lee, Reversible redox reactions in an epitaxially stabilized $SrCoO_x$ oxygen sponge, Nat. Mater. **12**, 1057 (2013).

[15] J. B. Goodenough, An interpretation of the magnetic properties of the perovskite-type mixed crystals $La_{1x}Sr_xCoO_{3-\lambda}$, J. Phys. Chem. Solids **6**, 287 (1958).

[16] J. B. Goodenough, Metallic oxides, Prog. Solid State Chem. **5**, 145 (1971).

[17] S. Sugano, Y. Tanabe, and H. Kamimura, *Multiplets of Transition-Metal Ions in Crystals* (Academic, New York, 1970), Chap. 5.

[18] R. H. Potze, G. A. Sawatzky, and M. Abbate, Possibility for an intermediate-spin ground state in the charge-transfer material $SrCoO_3$, Phys. Rev. B **51**, 11501 (1995).

[19] M. W. Haverkort, Z. Hu, J. C. Cezar, T. Burnus, H. Hartmann, M. Reuther, C. Zobel, T. Lorenz, A. Tanaka, N. B. Brookes, H.-H. Hsieh, H.-J. Lin, C.-T. Chen, and L. H. Tjeng, Spin State Transition in $LaCoO_3$ Studied Using Soft X-ray Absorption Spectroscopy and Magnetic Circular Dichroism, Phys. Rev. Lett. **97**, 176405 (2006).

[20] J.-M. Chen, Y.-Y. Chin, M. Valldor, Z. Hu, J.-M. Lee, S.-C. Haw, N. Hiraoka, H. Ishii, C.-W. Pao, K.-D. Tsuei, J.-F. Lee, H.-J. Lin, L.-Y. Jang, A. Tanaka, C.-T. Chen, and L. H. Tjeng, A complete high-to-low spin state transition of trivalent cobalt ion in octahedral symmetry in $SrCo_{0.5}Ru_{0.5}O_{3-\delta}$, J. Am. Chem. Soc. **136**, 1514 (2014).

[21] X. Ou, F. Fan, Z. Li, H. Wang, and H. Wu, Spin-state transition induced half metallicity in a cobaltate from first principles, Appl. Phys. Lett. **108**, 092402 (2016).

[22] H. Taguchi, Y. Takeda, F. Kanamaru, M. Shimada and M. Koizumi, Barium Cobalt Trioxide, Acta Crystallogr., Sect. B **33**, 1298 (1977).

[23] N. Raghu, V. Ravi, and T. R. N. Kutty, ZnO varistors with $BaCoO_{3-x}$ $(0.12 > x > 0)$ as the only formulating phase, Mater. Res. Bull. **26**, 261 (1991).

[24] K. Yamaura, H. W. Zandbergen, K. Abe, and R. J. Cava, Synthesis and properties of the structurally one-dimensional cobalt oxide $Ba_{1-x}Sr_xCoO_3$ $(0 \leqslant x \leqslant 0.5)$, J. Solid State Chem. **146**, 96 (1999).

[25] J. Sugiyama, H. Nozaki, J. H. Brewer, E. J. Ansaldo, T. Takami, H. Ikuta, and U. Mizutani, Appearance of a two-dimensional antiferromagnetic order in quasi-one-dimensional cobalt oxides, Phys. Rev. B **72**, 064418 (2005).

[26] J. Sugiyama, H. Nozaki, Y. Ikedo, K. Mukai, D. Andreica, A. Amato, J. H. Brewer, E. J. Ansaldo, G. D. Morris, T. Takami, and H. Ikuta, Evidence of Two Dimensionality in Quasi-One-Dimensional Cobalt Oxides, Phys. Rev. Lett. **96**, 197206 (2006).

[27] S. Hébert, V. Pralong, D. Pelloquin, and A. Maignan, Hexagonal perovskite cobaltites: Unconventional magnetism at low temperature, J. Magn. Magn. Mater. **316**, 394 (2007).

[28] N. Achiwa, Linear antiferromagnetic chains in hexagonal $ABCl_3$-Type compounds (A; Cs, or Rb, B; Cu, Ni, Co, or Fe), J. Phys. Soc. Jpn. **27**, 561 (1969).

[29] H. Nozaki, M. Janoschek, B. Roessli, J. Sugiyama, L. Keller, J. H. Brewer, E. J. Ansaldo, G. D. Morris, T. Takami, and H. Ikuta, Neutron diffraction and μSR study on the antiferromagnet $BaCoO_3$, Phys. Rev. B **76**, 014402 (2007).

[30] S. Agrestini, L. C. Chapon, A. Daoud-Aladine, J. Schefer, A. Gukasov, C. Mazzoli, M. R. Lees, and O. A. Petrenko, Nature of the Magnetic Order in $Ca_3Co_2O_6$, Phys. Rev. Lett. **101**, 097207 (2008).

[31] C. L. Fleck, M. R. Lees, S. Agrestini, G. J. McIntyre, and O. A. Petrenko, Field-driven magnetization steps in $Ca_3Co_2O_6$: A single-crystal neutron-diffraction study, Europhys. Lett. **90**, 67006 (2010).

[32] S. Agrestini, C. L. Fleck, L. C. Chapon, C. Mazzoli, A. Bombardi, M. R. Lees, and O. A. Petrenko, Slow Magnetic Order-Order Transition in the Spin Chain Antiferromagnet $Ca_3Co_2O_6$, Phys. Rev. Lett. **106**, 197204 (2011).

[33] A. Maignan, V. Hardy, S. Hébert, M. Drillon, M. R. Lees, O. Petrenko, D. Mc K. Paul, and D. Khomskii, Quantum tunneling of the magnetization in the Ising chain compound $Ca_3Co_2O_6$, J. Mater. Chem. **14**, 1231 (2004).

[34] V. Hardy, M. R. Lees, O. A. Petrenko, D. McK. Paul, D. Flahaut, S. Hébert, and A. Maignan, Temperature and time dependence of the field-driven magnetization steps

in $Ca_3Co_2O_6$ single crystals, Phys. Rev. B **70**, 064424 (2004).

[35] T. Burnus, Z. Hu, H. Wu, J. C. Cezar, S. Niitaka, H. Takagi, C. F. Chang, N. B. Brookes, H.-J. Lin, L. Y. Jang, A. Tanaka, K. S. Liang, C. T. Chen, and L. H. Tjeng, X-ray absorption and x-ray magnetic dichroism study on Ca_3CoRhO_6 and Ca_3FeRhO_6, Phys. Rev. B **77**, 205111 (2008).

[36] J. Choi, H. T. Yi, S. Lee, Q. Huang, V. Kiryukhin, and S.-W. Cheong, Ferroelectricity in an Ising Chain Magnet, Phys. Rev. Lett. **100**, 047601 (2008).

[37] H. Wang, J. Yang, C. Dong, Q. Mao, J. Du, and M. Fang, Crystal growth and characterization of the quasi-one-dimensional compound $BaCoO_3$, J. Cryst. Growth **430**, 52 (2015).

[38] J. Zaanen, G. A. Sawatzky, and J. W. Allen, Band Gaps and Electronic Structure of Transition-Metal Compounds, Phys. Rev. Lett. **55**, 418 (1985).

[39] J. L. Cacheiro, M. Iglesias, V. Pardo, D. Baldomir, and J. Arias, Possible spin configurations and magnetism in $BaCoO_3$ perovskite, Int. J. Quantum Chem. **91**, 252 (2003).

[40] V. Pardo, P. Blaha, M. Iglesias, K. Schwarz, D. Baldomir, and J. E. Arias, Magnetic structure and orbital ordering in $BaCoO_3$ from first-principles calculations, Phys. Rev. B **70**, 144422 (2004); **75**, 059902(E) (2007).

[41] V. Pardo, P. Blaha, M. Iglesias, D. Baldomir, K. Schwarz, M. Pereiro, J. Botana, and J. E. Arias, Bandstructure study of magnetic and orbital order in $BaCoO_3$, J. Magn. Magn. Mater. **290**, 349 (2005).

[42] V. Pardo, D. Baldomir, J. Rivas, J. Castro, and J. E. Ariasb, Orbital and magnetic structure of quasi-1D cobaltites: *Ab initio* calculations and experiment, J. Magn. Magn. Mater. **300**, 48 (2006).

[43] V. Pardo, P. Blaha, K. Schwarz, and D. Baldomirab, Possible non-collinear magnetic configurations in $BaCoO_3$, Phys. B (Amsterdam, Neth.) **378**, 556 (2006).

[44] V. Pardo, P. Blaha, R. Laskowski, D. Baldomir, J. Castro, K. Schwarz, and J. E. Arias, Ising-type behavior in the antiferromagnetic phase of $BaCoO_3$ from first principles, Phys. Rev. B **76**, 165120 (2007).

[45] C. Felser, K. Yamaura, and R. J. Cava, The electronic structure of hexagonal $BaCoO_3$, J. Solid State Chem. **146**, 411 (1999).

[46] G. Jackeli and G. Khaliullin, Mott Insulators in the Strong Spin-Orbit Coupling Limit: From Heisenberg to a Quantum Compass and Kitaev Models, Phys. Rev. Lett. **102**, 017205 (2009).

[47] J. Chaloupka, G. Jackeli, and G. Khaliullin, Kitaev-Heisenberg Model on a Honeycomb Lattice: Possible Exotic Phases in Iridium Oxides A_2IrO_3, Phys. Rev. Lett. **105**, 027204 (2010).

[48] A. Kitaev, Anyons in an exactly solved model and beyond, Ann. Phys. (NY) **321**, 2 (2006).

[49] K. I. Kugel, D. I. Khomskii, A. O. Sboychakov, and S. V. Streltsov, Spin-orbital interaction for face-sharing octahedra: Realization of a highly symmetric SU(4) model, Phys. Rev. B **91**, 155125 (2015).

[50] D. I. Khomskii, K. I. Kugel, A. O. Sboychakov, and S. V. Streltsov, Role of local geometry in the spin and orbital structure of transition metal compounds, J. Exp. Theor. Phys. **122**, 484 (2016).

[51] K. I. Kugel and D. I. Khomskii, Crystal structure and magnetic properties of substances with orbital degeneracy, Zh. Eksp. Teor. Fiz. **64**, 1429 (1973) [Sov. Phys.-JETP **37**, 725 (1973)].

[52] K. I. Kugel and D. I. Khomskii, The Jahn-Teller effect and magnetism: Transition metal compounds, Usp. Fiz. Nauk **136**, 621 (1982) [Sov. Phys. Usp. **25**, 231 (1982)].

[53] B. Frischmuth, F. Mila, and M. Troyer, Thermodynamics of the One-Dimensional SU(4) Symmetric Spin-Orbital Model, Phys. Rev. Lett. **82**, 835 (1999).

[54] H.-J. Lin, Y. Y. Chin, Z. Hu, G. J. Shu, F. C. Chou, H. Ohta, K. Yoshimura, S. Hébert, A. Maignan, A. Tanaka, L. H. Tjeng, and C. T. Chen, Local orbital occupation and energy levels of Co in Na_xCoO_2: A soft x-ray absorption study, Phys. Rev. B **81**, 115138 (2010).

[55] Z. Hu, H. Wu, M. W. Haverkort, H. H. Hsieh, H.-J. Lin, T. Lorenz, J. Baier, A. Reichl, I. Bonn, C. Felser, A. Tanaka, C. T. Chen, and L. H. Tjeng, Different Look at the Spin State of Co^{3+} Ions in a CoO_5 Pyramidal Coordination, Phys. Rev. Lett. **92**, 207402 (2004).

[56] Z. Hu, H. Wu, T. C. Koethe, S. N. Barilo, S. V. Shiryaev, G. L. Bychkov, C. Schler-Langeheine, T. Lorenz, A. Tanaka, H. H. Hsieh, H. J. Lin, C. T. Chen, N. B. Brookes, S. Agrestini, Y. Y. Chin, M. Rotter, and L. H. Tjeng, Spin-state order/disorder and metal-insulator transition in $GdBaCo_2O_{5.5}$: Experimental determination of the underlying electronic structure, New J. Phys. **14**, 123025 (2012).

[57] C. Mitra, Z. Hu, P. Raychaudhuri, S. Wirth, S. I. Csiszar, H. H. Hsieh, H.-J. Lin, C. T. Chen, and L. H. Tjeng, Direct observation of electron doping in $La_{0.7}Ce_{0.3}MnO_3$ using x-ray absorption spectroscopy, Phys. Rev. B **67**, 092404 (2003).

[58] Z. Hu, G. Kaindl, A. Hayer, and D. Reinen, XANES spectroscopy on ceramic oxides of chromium, cobalt, and nickel in various oxidation states and its relevance with regard to chemical bonding, Z. Anorg. Allg. Chem. **627**, 2647 (2001).

[59] W. B. Wu, D. J. Huang, J. Okamoto, A. Tanaka, H.-J. Lin, F. C. Chou, A. Fujimori, and C. T. Chen, Orbital Symmetry and Electron Correlation in Na_xCoO_2, Phys. Rev. Lett. **94**, 146402 (2005).

[60] T. Mizokawa, Y. Wakisaka, T. Sudayama, C. Iwai, K. Miyoshi, J. Takeuchi, H. Wadati, D. G. Hawthorn, T. Z. Regier, and G. A. Sawatzky, Role of Oxygen Holes in $LixCoO_2$ Revealed by Soft X-Ray Spectroscopy, Phys. Rev. Lett. **111**, 056404 (2013).

[61] J. Okamoto, H. Miyauchi, T. Sekine, T. Shidara, T. Koide, K. Amemiya, A. Fujimori, T. Saitoh, A. Tanaka, Y. Takeda, and M. Takano, Role of oxygen holes in Li_xCoO_2 revealed by soft x-ray spectroscopy, Phys. Rev. B **62**, 4455 (2000).

[62] C. de la Calle, J. A. Alonso, and M. T. Fernández-Díaz, Polymorphism of $Ba_{1-x}Sr_xCoO_{3-\delta}$ ($0 \leqslant x \leqslant 1$) perovskites: A thermal and structural study by neutron diffraction, Z. Naturforsch. **63b**, 647 (2008).

[63] P. Bezdicka, A. Wattiaux, J. C. Grenier, M. Pouchard, and P. Hagenmuller, Preparation and characterization of fully stoichiometric $SrCoO_3$ by electrochemical oxidation, Z. Anorg. Allg. Chem. **619**, 7 (1993).

[64] J. Kuneš, V. Křápek, N. Parragh, G. Sangiovanni, A. Toschi, and A. V. Kozhevnikov, Spin State of Negative Charge-Transfer Material $SrCoO_3$, Phys. Rev. Lett. **109**, 117206 (2012).

[65] J. Matsuno, Y. Okimoto, Z. Fang, X. Z. Yu, Y. Matsui, N. Nagaosa, M. Kawasaki, and Y. Tokura, Metallic Ferromagnet with Square-Lattice CoO_2 Sheets, Phys. Rev. Lett. **93**, 167202 (2004).

[66] K.-W. Lee and W. E. Pickett, Correlation effects in the high formal oxidation-state compound Sr_2CoO_4, Phys. Rev. B **73**, 174428 (2006).

[67] A. Tanaka and T. Jo, Resonant 3d, 3p and 3s photoemission in transition metal oxides predicted at 2p threshold, J. Phys. Soc. Jpn. **63**, 2788 (1994).

[68] F. M. F. de Groot, Z. W. Hu, M. F. Lopez, G. Kaindl, F. Guillot, and M. Tronc, Differences between L_3 and L_2 x-ray absorption spectra of transition metal compounds, J. Chem. Phys. **101**, 6570 (1994).

[69] The LS, IS, and HS state XAS/XMCD spectra from Fig. 3 were all calculated using the same $Co^{4+}O_6$ cluster with parameters chosen such that the LS forms the ground state. The spectra were then calculated starting from the lowest LS, lowest IS, and lowest HS states. The following parameters values were used: Coulomb energies $U_{3d3d} = 5.0$ eV and $U_{3d2p} = 6.0$ eV; O $2p$ to Co $3d$ charge transfer energy $\triangle_{CT} = -3.5$ eV; Slater-Koster transfer integral $pd\sigma = -1.345$ eV. The Slater integrals F^2 and F^4 are reduced to 70% of the atomic values. For one hole occupying the e_g^π orbital in the D_{3d} local symmetry, $\triangle D_{3d} = -0.6$ eV, and $10Dq = 0.7$ eV. For the case with a local distortion of the CoO_6 octahedron having a monoclinic C_{2h} or lower symmetry, $\triangle D_{3d} = -0.2$ eV, mixing term $V_{\text{mix}} = -0.7$ eV, and $\triangle e_g^\pi = 0.19$ eV. See also Lin *et al.* [54] for further details of the definitions.

[70] T. K. Sham, X-ray absorption spectra of ruthenium L edges in $Ru(NH_3)_6Cl_3$, J. Am. Chem. Soc. **105**, 2269 (1983).

[71] Z. Hu, H. von Lips, M. S. Golden, J. Fink, G. Kaindl, F. M. F. de Groot, S. Ebbinghaus, and A. Reller, Multiplet effects in the Ru $L_{2,3}$ x-ray-absorption spectra of Ru(IV) and Ru(V) compounds, Phys. Rev. B **61**, 5262 (2000).

[72] A. Tanaka, Electronic structure and phase transition in V_2O_3: Importance of 3d spin-orbit interaction and lattice distortion, J. Phys. Soc. Jpn. **71**, 1091 (2002).

[73] M. W. Haverkort, Spin and orbital degrees of freedom in transition metal oxides and oxide thin films studied by soft x-ray absorption spectroscopy, Ph.D. thesis, University of Cologne, 2005.

[74] B. T. Thole, P. Carra, F. Sette, and G. van der Laan, X-ray Circular Dichroism as a Probe of Orbital Magnetization, Phys. Rev. Lett. **68**, 1943 (1992).

[75] P. Carra, B. T. Thole, M. Altarelli, and X. Wang, X-ray Circular Dichroism and Local Magnetic Fields, Phys. Rev. Lett. **70**, 694 (1993).

[76] M.-H. Whangbo, H.-J. Koo, D. Dai, and A. Villesuzanne, Analysis of the electron localization, the anisotropy of electrical conductivity, the orbital ordering, and spin-exchange interactions in $BaVS_3$ on the basis of first principles and semi-empirical electronic structure calculations, J. Solid State Chem. **165**, 345 (2002).

[77] D. Louca and J. L. Sarrao, Dynamical Disorder of Spin-Induced Jahn-Teller Orbitals with the Insulator-Metal Transition in Cobaltites, Phys. Rev. Lett. **91**, 155501 (2003).